C6_12_ISCS 2012

by Pranowo Pranowo

Submission date: 08-Jan-2018 02:01AM (UTC+0700)
Submission ID: 900721218
File name: C6_12_ISCS_2012.doc (4.34M)
Word count: 1853
Character count: 11996

Numerical Simulation Of Interaction Of Ultrasonic Wave With Bone

Pranowo
Teknik Informatika Universitas Atma Jaya Yogyakarta
Jl. Babarsari 43 Yogyakarta 55281 Indonesia
Email: pran@staff.uajy.ac.id

ABSTRACT
Better understanding of the mechanism in which ultrasonic wave interacts with bone is important in therapy and diagnosis alike, such as extracorporeal shock wave therapy (ESWT). In this paper, numerical simulation for investigating the interaction of ultrasonic wave with bone is presented. The elastodynamic equations was used as the governing equations. A nodal high order discontinuous galerkin finite element was used for the spatial discretization while an explicit low storage fourth order Runge Kutta scheme is used to march in the time domain. This paper demostrated the power of numerical method for biomedical research, which deals with ultrasonic wave propagation in human body.

Keywords: ultrasonic wave, bone, discontinuous galerkin

1. INTRODUCTION
Interaction between ultrasonic wave propagation with bone occurs in many biomedical treatments, such as extracorporeal shock wave therapy (ESWT). The ESWT is a noninvasive treatment for a variety of musculoskeletal ailments.The ultrasonic shock wave is generated by a spark plug source (lithotripter) in water and then focused using an acoustic lens or reflector so the energy of the wave is concentrated in a small treatment region (Fagnan, 2010).

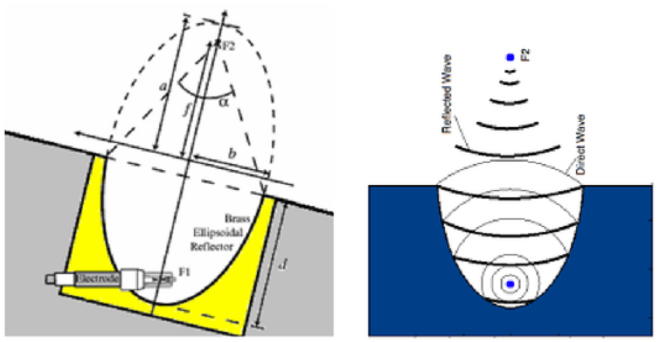

Figure1. Lithotripter

Better understanding of the mechanism of the interaction of the ultrasonic wave with bone is important for the biomedical treatment. In this paper, numerical simulation approach for investigating the mechanism was proposed.. The bone was assumed as elastic solid material and the water as inviscid fluid. The water can be treated as solid with zero shear stress. Therefor a single partial differential equation system, called elastodynamics equations, can be applied as the governing equations for both materials. Then the governing equations is formulated in terms of velocity-stress in both media. Many numerical method were proposed for the solution of the governing equations [e.g., finite difference time domain (FDTD) or finite element methods (FEM)]. The FDTD method (Kaufmann et al., 2008; Matsukawa et al., 2008) is limited for simple spatial domain only and the conventional FEM (Protopappas et al., 2007; Nguyen et al., 2010) has a high dispersion error. A nodal high order discontinuous galerkin (DG) finite element is used for the spatial discretization while an explicit low storage fourth order Runge Kutta scheme is used to march in the time domain. The DG method can apllied for irregular domain and has low dispersion error.

The simulation of ultrasonic wave by discontinuous galerkin method in unbounded domains requires a specific boundary condition of the necessarily truncated computational domain. We propose an absorbing boundary condition called perfectly matched layer (PML). Presented in time domain electromagnetic simulations (Berenger, 1996), PML has since been used extensively in that field. PML has also been incorporated into a variety of wave propagation algorithms. Colino and Tsogka (2001) have formulated and demonstrated PML in the P-SV case via Virieux (1986) finite difference scheme and a mixed finite element algorithms.

2. GOVERNING EQUATIONS

Starting with the system of governing equations, each equation is split into a parallel and perpendicular component, based on spatial derivative separation. That is, the perpendicular equations contains the spatial derivative term which acts normal to the coordinate plane of interest and a damping term, and the parallel equation contain the remaining spatial derivative terms. Finally, an additional equation is required to sum the results of the split equations

$$
\begin{aligned}
&\frac{\partial v_{xx}}{\partial t}+\sigma(x)v_{xx}=\frac{1}{\rho}\frac{\partial \tau_{xx}}{\partial x}+f_x \quad ; \quad \frac{\partial v_{xy}}{\partial t}+\sigma(y)v_{xy}=\frac{1}{\rho}\frac{\partial \tau_{xy}}{\partial y}\\
&\frac{\partial v_{yx}}{\partial t}+\sigma(x)v_{yx}=\frac{1}{\rho}\frac{\partial \tau_{xy}}{\partial x} \quad ; \quad \frac{\partial v_{yy}}{\partial t}+\sigma(y)v_{yy}=\frac{1}{\rho}\frac{\partial \tau_{yy}}{\partial y}+f_y\\
&\frac{\partial \tau_{xxx}}{\partial t}+\sigma(x)\tau_{xxx}=(\lambda+2\mu)\frac{\partial v_x}{\partial x} \quad ; \quad \frac{\partial \tau_{xxy}}{\partial t}+\sigma(y)\tau_{xxy}=\lambda\frac{\partial v_y}{\partial y}\\
&\frac{\partial \tau_{yyx}}{\partial t}+\sigma(x)\tau_{yyx}=\lambda\frac{\partial v_x}{\partial x} \quad ; \quad \frac{\partial \tau_{yyy}}{\partial t}+\sigma(y)\tau_{yyy}=(\lambda+2\mu)\frac{\partial v_y}{\partial xy}\\
&\frac{\partial \tau_{xyx}}{\partial t}+\sigma(x)v_{xyx}=\mu\frac{\partial v_y}{\partial x} \quad ; \quad \frac{\partial \tau_{xyy}}{\partial t}+\sigma(y)v_{xyy}=\mu\frac{\partial v_x}{\partial y}
\end{aligned}
\tag{1}
$$

$$v_x=v_{xx}+v_{xy}\ ,\ v_y=v_{yx}+v_{yy}\ ,\ \tau_{xx}=\tau_{xxx}+\tau_{xxy}\ ,\ \tau_{yy}=\tau_{yyx}+\tau_{yyy},\ \tau_{xy}=\tau_{xyx}+\tau_{xyy}$$

In the absorbing layers we use the following model for the damping parameters:

$$\sigma(x)=d_0\left(\frac{x}{\delta}\right)^2 \ ;\ \sigma(y)=d_0\left(\frac{y}{\delta}\right)^2 \quad \text{and} \quad d_0=\log\left(\frac{1}{R}\right)\frac{3c_p}{2\chi}$$

where δ is the length of the layer and d_0 is a function of the theoretical reflection coefficient (R)

3. DISCONTINUOUS GALERKIN METHOD

For simplicity, the split equations (2) are writen in vector form as follows:

$$\frac{\partial \mathbf{q}}{\partial t}+\mathbf{A}\frac{\partial \mathbf{q}}{\partial x}+\mathbf{B}\frac{\partial \mathbf{q}}{\partial y}=\mathbf{f} \tag{2}$$

where $\mathbf{q}=[v_{xx}\quad v_{xy}\quad v_{yx}\quad v_{yy}\quad \tau_{xxx}\quad \tau_{xxy}\quad \tau_{yyx}\quad \tau_{yyy}\quad \tau_{xyx}\quad \tau_{xyy}]^T$

The spatial derivatives are discretized by using a discontinuous galerkin method. The simplified of Eq.(2) according to Galerkin's procedure using the same basis function ϕ within each element is defined below (Hesthaven & Warburton, 2002; 2008).

$$\left(\phi,\frac{\partial \mathbf{q}}{\partial t}+\mathbf{A}\frac{\partial \mathrm{q}}{\partial x}+\mathbf{B}\frac{\partial \mathrm{q}}{\partial y}\right)=0$$

$$\Leftrightarrow\left(\phi,\frac{\partial \mathrm{q}}{\partial t}\right)_{\Omega}+\left(\phi,\mathbf{A}n_x\mathbf{q}+Bn_y\,\mathrm{q}\right)_{\partial\Omega}-\left(\frac{\partial}{\partial x}(\mathbf{A}\phi),\mathrm{q}\right)_{\partial\Omega}-\left(\frac{\partial}{\partial y}(\mathbf{B}\phi),\mathbf{q}\right)_{\Omega}=0 \qquad (3)$$

Here $(.,.)$ represents the normal 2 L inner product, the second term is flux vector and (n_x, n_y) are normal vector. The mathematical manipulation of the flux vector is calculated as below:

$$\left(\phi,\frac{\partial \mathrm{q}}{\partial t}+\mathbf{A}\frac{\partial \mathrm{q}}{\partial x}+\mathbf{B}\frac{\partial \mathrm{q}}{\partial y}\right)_{\Omega}+\left(\phi,\mathbf{A}n_x+\mathbf{B}n_y\right)\left(\hat{\mathrm{q}}-\mathrm{q}^-\right)_{\partial\Omega}=0$$

(5)

where $\mathbf{q}^-\big|_{\partial\Omega}=\hat{\mathbf{q}}^-\left(\mathbf{q}^-,\mathbf{q}^+\right)\big|_{\partial\Omega}$ and the last term of equation (3) is called numerical flux.

Here, we took the Kornwinder Dubiner function on straight sided triangle as the basis written in equation 4 (see Figs. 1 and 2):

$$\phi_{ij}(r,s)=\sqrt{\frac{2i+1}{2}}\sqrt{\frac{2i+2j+2}{2}}P_i^{0,0}\left(\frac{2(1+r)}{(1-s)}-1\right)P_j^{2=+1,0}(s) \qquad (4)$$

where, $P^{\alpha,\beta}$ is orthogonal Jacobi polynomial
All straight sided triangles are the image of this triangle under the map:

$$\begin{pmatrix}x\\y\end{pmatrix}=-\left(\frac{r+s}{2}\right)\begin{pmatrix}v_x^1\\v_y^1\end{pmatrix}+\left(\frac{1+r}{2}\right)\begin{pmatrix}v_x^2\\v_y^2\end{pmatrix}+\left(\frac{1+s}{2}\right)\begin{pmatrix}v_x^3\\v_y^3\end{pmatrix} \qquad (5)$$

The set of points in the triangle, which we can build the Lagrange interpolating polynomials, can be viewed as Gauss-Legendre –Lobatto (GLL) points.

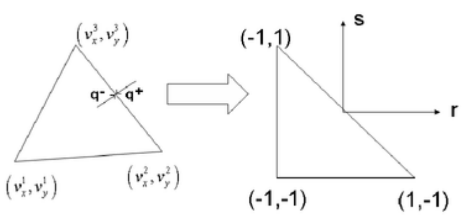

Figure 2: Coordinate Transformation

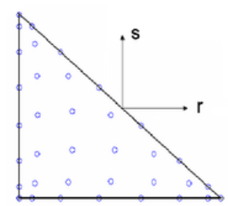

Figure 3: Seventh Order Gauss Lobatto Quadrature Nodes

The vector $\mathbf{q}$ is expanded using equation (4), we take expansion of v_x as example:

$$v_x(r,s)=\sum_{i=0}^{N}\sum_{j=0}^{N-i}\phi_{ij}(r,s)\hat{v}_{xij} \qquad (6)$$

$$v_x(r_n,s_n)=\sum_{m=1}^{m=M}\mathbf{V}_{nm}\hat{v}_{xm}$$

$$\hat{v}_{xm}=\sum_{m=1}^{m=M}\left(\mathbf{V}^{-1}\right)_{mj}v_x(r_j,s_j) \qquad (7)$$

$$\frac{\partial v_x}{\partial r}(r,s)=\sum_{i=0}^{N}\sum_{j=0}^{N-i}\frac{\partial \phi_{ij}}{\partial r}(r,s)\hat{v}_{xij}=\hat{\mathrm{D}}^r\mathbf{V}^{-1}v_x(r,s) \qquad \hat{\mathbf{D}}^r=\frac{\partial \phi}{\partial r}$$
$$\frac{\partial v_x}{\partial s}(r,s)=\sum_{i=0}^{N}\sum_{j=0}^{N-i}\frac{\partial \phi_{ij}}{\partial s}(r,s)\hat{v}_{xij}=\hat{\mathrm{D}}^s\mathbf{V}^{-1}v_x(r,s) \quad ; \quad \hat{\mathbf{D}}^s=\frac{\partial \phi}{\partial s}$$

where $\mathbf{V}_{ij}$ and N are Vandermonde matrix dan the order of Jacobi polynomial respectively.
The semi discrete Eq. (3) is integrated in time marching by using five stage of fourth order 2N-storage Runge-Kutta scheme as developed by Carpenter & Kennedy (1994). The final equations are found as written in Eq. (8).

$$\frac{d\mathbf{q}}{dt}=L[t,\mathbf{q}(t)] \tag{8}$$

$$d\mathbf{q}_j=A_j d\mathbf{q}_{j-1}+dtL(\mathbf{q}_j)$$
$$\mathbf{q}_j=\mathbf{q}_{j-1}+B_j+d\mathbf{q}_j$$

where dt is the time step. The vectors A and B are the coefficients that will be used to determine the properties of the scheme. The maximum time step is (Hesthaven and Warburton, 2002):

$$\Delta t \le \frac{2h}{c_p(N-1)^2} \tag{9}$$

where c_p is primary wave velocity and h is the smallest edge length of the element

4. RESULTS AND DISCUSSIONS

In this section we present two numerical examples. The the first example aims at showing the accuracy of DGM compared to analytical solution and Fem whis proposed by Diaz and Patrick (2005) and the second example aims at showing that DGM can easily handle problems with complicated interface.

4.1. Numerical Example I

The first example has a simple configuration: two half-planes separated by a straight interface, one constitutes the fluid medium and the second one constitutes solid medium. The material properties for the fluid are $c_p = 1500\,\mathrm{ms}^{-1}$, $c_s = 0\,\mathrm{ms}^{-1}$ and $\rho = 1000\ \mathrm{kg\ m}^{-3}$ and the material properties for the solid are $c_p = 4000\,\mathrm{ms}^{-1}$, $c_s = 1800\ \mathrm{ms}^{-1}$ and $\rho = 1850\ \mathrm{kg\ m}^{-3}$. The size of each medium is 20 mm × 5 mm. We added absorbing layer surounding the domain with the thickness of the layer equals 1 mm and total number of triangular elements is 15060. The polynomial degree is $N = 3$ and the time step $\Delta t = 10^{-8}\,s$. The source function is a point source located in the fluid at 2 mm above the interface, the time variation of the source is given as Gaussian with dominating frequency is 1 MHz. Snapshots of the first example can be seen in figure 4a – 4b.

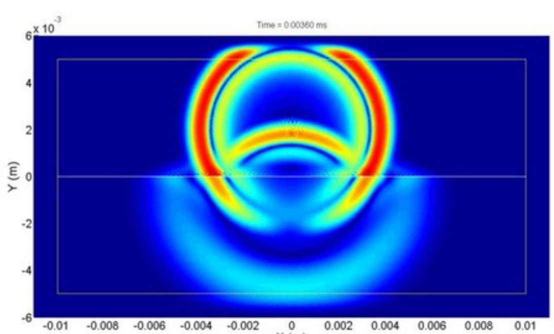

Figure 4a: Velocity fields of 1st example at 0.36 μs

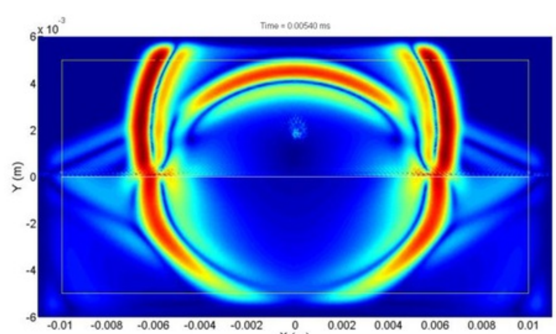

Figure 4b: Velocity fields of 1st example at 0.54 μs

To validate the DG method, we compare the numerical DGM (the green curve) solution to the FEM solution (the red curve) and analytical solution (the blue curve) which are provided by Diaz and Patrick. (2005). The two components of the numerical and analytical velocity are shown by figure 5a and 5b. The curves are perfectly superimposed, showing the goood accuracy of DGM. From 4b we can see no reflection on the left, right and bottom edges. The PML absorbed the outgoing waves well.

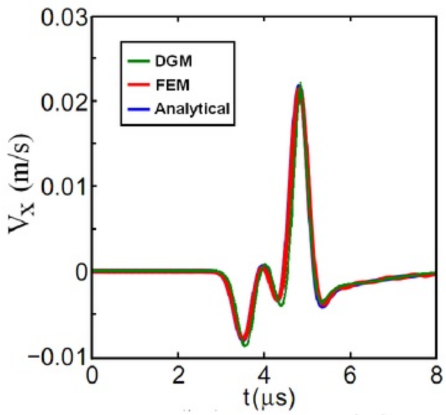

Figure 5a: Horizontal velocity (v_x)

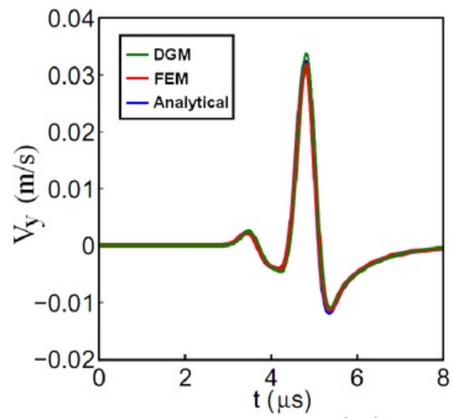

Figure 5b: Vertical velocity (v_y)

4.2. Numerical Example II

In this example, the interaction of ultrasonic wave propagation, which generated by lithotripter, with human skull. The contour of human skull was extracted from MRI scanned image by using level set segmentation, as shown in figure 6. Figure 7 shown the whole of physical domain, including lithotripter and absorbing layer. The major and minor axes of the ellipsoid of the lithotripter are $a = 70$ mm and $b =$ 40 mm. The domain is dicretized into triangular 7433 elements. The material properties for the water are $\mu = 0\,\text{GPa}$, $\lambda = 2.2\,\text{GPa}$ and $\rho = 1000$ kg m^{-3} and the material properties for the bone are $\mu = 9.4\,\text{GPa}$, $\lambda = 20\,\text{GPa}$ and $\rho = 2000$ kg m^{-3}. The polynomial degree is $N = 4$ and the time step $\Delta t = 10^{-8}\,s$. The source function is a point source located at the focus of ellipsoid, the time variation of the source is given as Ricker (i.e., the first derivative of a Gaussian) with dominating frequency is 0.5 MHz.

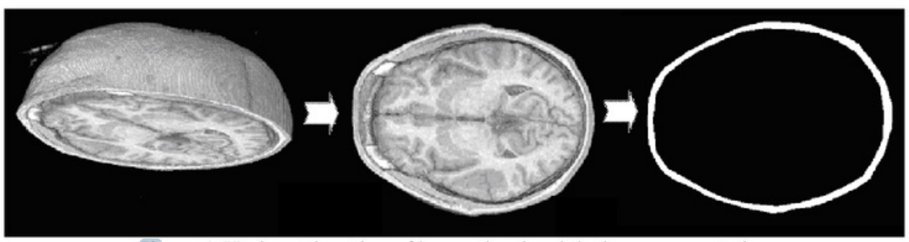

Figure 6. Horizontal section of human head and the bone segmentation (https://www.msu.edu/~brains/brains/human/horizontal/1400_cut.html)

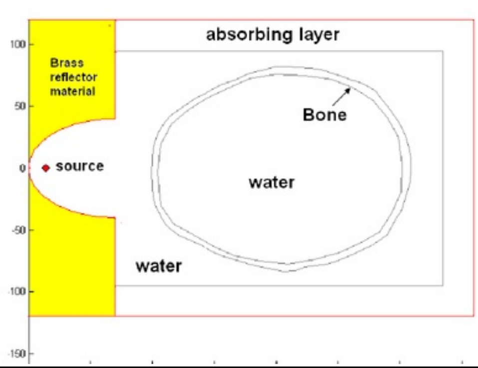

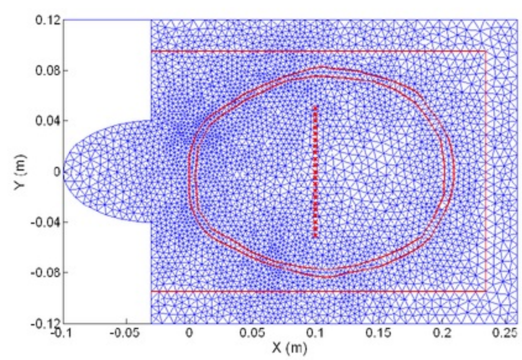

Figure 9a – 9h show the interaction ultrasonic wave propagation with the human skull at $t = 20,\ t = 50,\ t = 70,\ t = 90,\ t = 120,,\ t = 140,\ t = 160$ and $t = 200\ \mu s$. The wave propagation starts from the focus of the ellipsoid. The wave, which hit the the metal wall, will be reflected back. The metal wall acts as wave guide, so the wave will be guided to propagate to the right. When the wave encounters the bone, the wave will be scattered and partially will be transmitted through the bone. Figure 9c and figure 9d show the scattered and transmitted waves at the interface clearly. The transmitted wave will be guided along the bone and propagates faster than the wave that propagates in the water (figure 9d - 9h). The outgoing wave that left the domain will be absorbed well in the PML.

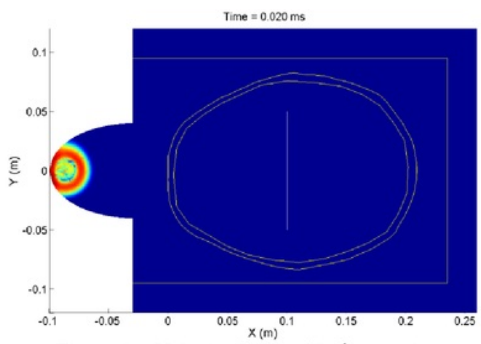

Figure 9a: Velocity fields of 2 nd example at 20 μs

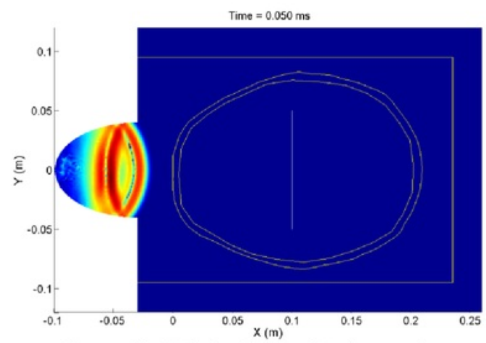

Figure 9b: Velocity fields of 2 nd example at 50 μs

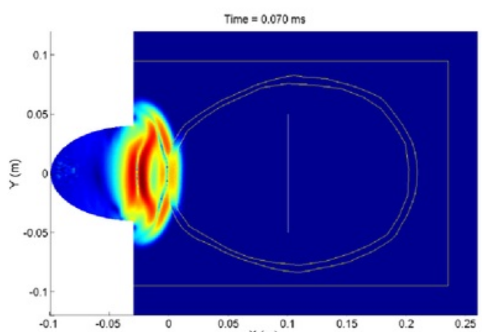

Figure 9c: Velocity fields of 2 nd example at 70 μs

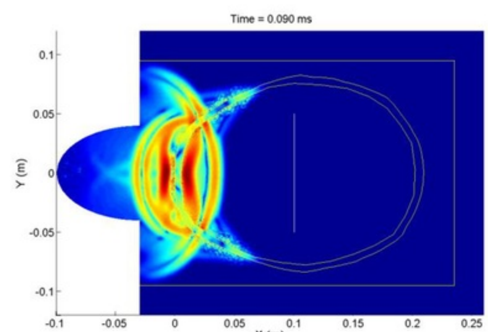

Figure 9d: Velocity fields of 2 nd example at 090 μs

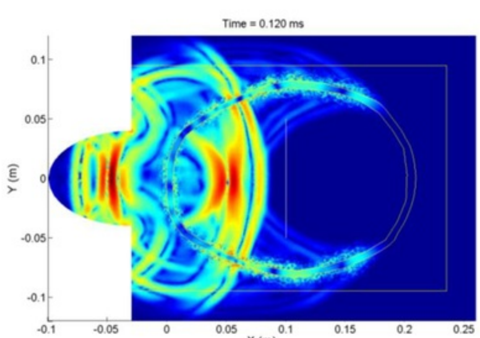

Figure 9e: Velocity fields of 2 nd example at 120 μs

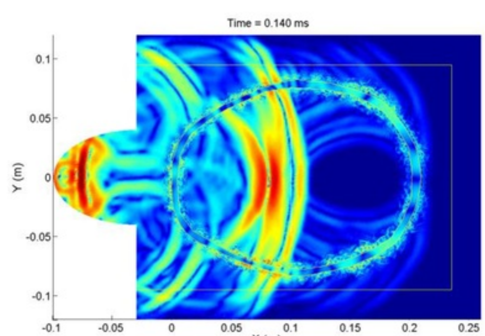

Figure 9f: Velocity fields of 2 nd example at 140 μs

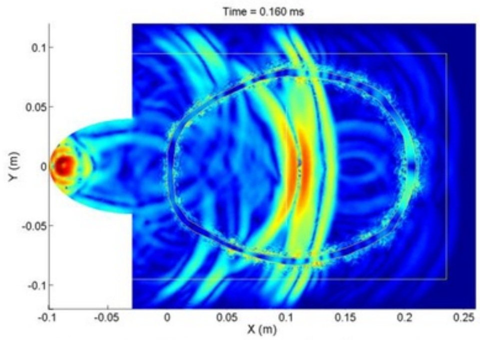

Figure 9g: Velocity fields of 2 nd example at 160 μs

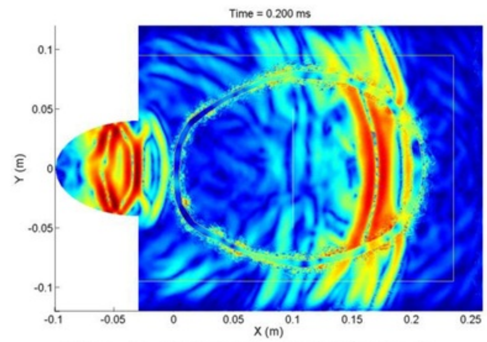

Figure 9h: Velocity fields of 2 nd example at 200 μs

Figure 10.a and 10.b contain the traces recorded at receiver position = (0.1, 0.05), and figure 10.c contains the traces recorded at all receiver position. As one can see from the figurer, the solutions obtained from discontinuous galerkin methods has smooth solution contained no numerical oscillation.

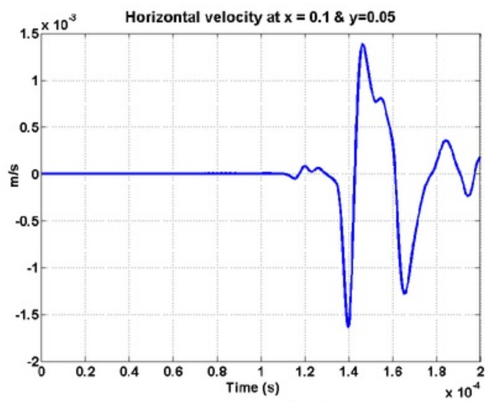

Figure 10a: Horizontal velocity (v_x) recorded at receiver position x =0.1 and y = 0.05 m

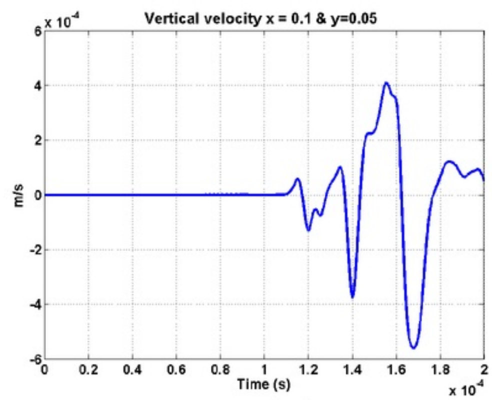

Figure 10b: Vertical velocity (v_x) at receiver position x =0.1 and y = 0.05 m

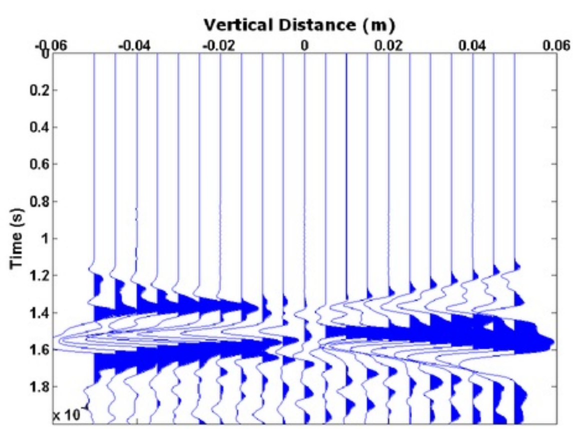

4.3. Conclusions

In this paper, numerical simulation for investigating the interaction of ultrasonic wave with bone based on discontinuous galerkin method is presented. To model the interaction ultrasonic wave with bone, bone material was considered as a elastic solid medium immersed in an acoustic fluid. The discontinuous galerkin method provides stable and accurate methods for simulating the interaction ultrasonic wave with bone. It is shown that numerical simulation is a valuable tool for investigating ultrasonic wave interactions with bone. Numerical simulation can provide important insights that can lead to many practical advantages, dealing with ultrasonic wave propagation in human body.

REFERENCES

Berenger, J. P. (1996). Three-Dimensional Perfectly Matched Layer for the Absorption of Electromagnetic Waves. Journal Computational Physics, 127, pp. 1363-379.

Carpenter, M. H.; and Kennedy, C. A. (1994). Fourth-order 2N-Storage Runge-Kutta Schemes. NASA Technical Memorandum 109112, NASA Langley Research Center, Hampton, Virginia.

Collino, F.; and Tsogka, C. (2001), Application of the PML absorbing layer model to the linear elastodynamic problem in anisotropic heterogeneous medium. Geophysical Journal International, Vol. 66, No. 1, pp. 294-307, 2001

Diaz, J.; and Patrick, J. (2005). Robust high order non-conforming finite element formulation for time domain fluid-structure interaction. Journal of Computational Acoustics, World Scientific, 13 (3), pp. 403-431.

Fagnan, K. M.. (2010). High-resolution Finite Volume Methods for Extracorporeal Shock Wave Therapy. Ph.D. Thesis. University of Washington .

Hesthaven, J. S.; and Warburton, T. (2002). High-order Nodal Methods on Unstructured Grids, I. Time Domain Solution of Maxwell's Equation. J. Computational Physics, 181, pp. 1-34.

Hesthaven, J. S.; and Warburton, T. (2008). Nodal Discontinuous Galerkin Methods: Algorithms, Analysis, and Applications, Springer, New York.

Kaufman, J.J., Gangming, L., and Siffert, R. S. (2008). Ultrasound Simulation in Bone. IEEE Transactions on Ultrasonics, Ferroelectrics, And Frequency Control, Vol. 55, No. 6, June 2008

Matsukawa, M., Mizuno, K., and Nagata, Y. (2008). The fast wave propagatin in bovine cancelous bone-experiments and simulation. The European Acoustics Association Conference, June 29 – July 4, 2008, Paris, France..

Nguyen, V. H., Naili, S., and Sansalone, V. (2010). Simulation of ultrasonic wave propagation in anisotropic cancellous bone immersed in fluid. Wave Motion, Volume 47, Issue 2, March 2010, Pages 117-129.

Protopappas, V.C. et al. (2007). Three-dimensional finite element modeling of guided ultrasound wave propagation in intact and healing long bones. J. Acoust. Soc. Am. 121 (6) June 2000.

C6_12_ISCS 2012

GRADEMARK REPORT

FINAL GRADE

/0

GENERAL COMMENTS

Instructor

PAGE 1

PAGE 2

PAGE 3

PAGE 4

PAGE 5

PAGE 6

PAGE 7

PAGE 8

C6_12_ISCS 2012

ORIGINALITY REPORT

19%	9%	13%	0%
SIMILARITY INDEX	INTERNET SOURCES	PUBLICATIONS	STUDENT PAPERS

PRIMARY SOURCES

1	Carey Marcinkovich. "On the implementation of perfectly matched layers in a three-dimensional fourth-order velocity-stress finite difference scheme", Journal of Geophysical Research, 2003 Publication	5%
2	hal.inria.fr Internet Source	2%
3	arxiv.org Internet Source	2%
4	JULIEN DIAZ. Journal of Computational Acoustics, 2005 Publication	1%
5	faraday.fc.up.pt Internet Source	1%
6	www.lrbo.ru Internet Source	<1%
7	COMPEL: The International Journal for Computation and Mathematics in Electrical and	<1%

Electronic Engineering, Volume 33, Issue 1-2 (2014-03-28)
Publication

8	www.prep4usmle.com Internet Source	<1%
9	Hesthaven, J.S.. "Spectral Collocation Time-Domain Modeling of Diffractive Optical Elements", Journal of Computational Physics, 19991101 Publication	<1%
10	Journal of Financial Reporting and Accounting, Volume 13, Issue 1 (2015) Publication	<1%
11	Jingyi Chen. "Application of the nearly perfectly matched layer for seismic wave propagation in 2D homogeneous isotropic media : Application of the nearly perfectly matched layer", Geophysical Prospecting, 07/2011 Publication	<1%
12	www.wessex.ac.uk Internet Source	<1%
13	fti.uajy.ac.id Internet Source	<1%
14	Jiang, L.. "Flow field of a triple-walled gas-sampling probe with sub-cooled boiling effect", Flow Measurement and Instrumentation,	<1%

200706
Publication

15	digital.lib.washington.edu Internet Source	<1%
16	Vu-Hieu Nguyen. "Simulation of ultrasonic wave propagation in anisotropic poroelastic bone plate using hybrid spectral/finite element method : ULTRASONIC WAVE PROPAGATION IN ANISOTROPIC POROELASTIC BONE PLATE", International Journal for Numerical Methods in Biomedical Engineering, 03/2012 Publication	<1%
17	people.na.infn.it Internet Source	<1%
18	COMPEL: The International Journal for Computation and Mathematics in Electrical and Electronic Engineering, Volume 33, Issue 4 (2014-09-16) Publication	<1%
19	lra.le.ac.uk Internet Source	<1%
20	Michael Dumbser. "An arbitrary high-order discontinuous Galerkin method for elastic waves on unstructured meshes ? II. The three-dimensional isotropic case", Geophysical Journal International, 10/2006 Publication	<1%

21	www.sdk.co.jp Internet Source		<1%
22	Encyclopedia of Earth Sciences Series, 2011. Publication		<1%
23	Machado, C.B.. "Experimental and simulation results on the effect of cortical bone mineralization in ultrasound axial transmission measurements: A model for fracture healing ultrasound monitoring", Bone, 20110501 Publication		<1%
24	Jean-Philippe Groby. "Seismic motion in urban sites consisting of blocks in welded contact with a soft layer overlying a hard half-space", Geophysical Journal International, 02/2008 Publication		<1%
25	Frank Natterer, Frank Wübbeling. "7. Nonlinear Tomography", Society for Industrial & Applied Mathematics (SIAM), 2001 Publication		<1%
26	Dolean, V.. "A domain decomposition method for solving the three-dimensional time-harmonic Maxwell equations discretized by discontinuous Galerkin methods", Journal of Computational Physics, 20080110 Publication		<1%